CrystEngComm

Accepted Manuscript

ROYAL SOCIETY OF CHEMISTRY

www.rsc.org/crystengcomm

Cite this: DOI: 10.1039/c0xx00000x

www.rsc.org/xxxxxx

ARTICLE TYPE

Mesoporous 3D ZnO-NiO architectures for high-performance supercapacitor electrode materials

ChengzhenWei,[a] Huan Pang, *[a, b] Cheng Cheng,[a] Junhong Zhao,[a] Pengwei Li [a] and Yongkang Zhang [a]

Received (in XXX, XXX) XthXXXXXXXXX 20XX, Accepted Xth XXXXXXXXX 20XX

DOI: 10.1039/b000000x

3D ZnO-NiO mesoporous architectures are synthesized through annealing the zinc hydroxide carbonate/nickel hydroxide carbonate composite precursor, which is prepared via a one-pot hydrothermal route. More importantly, we successfully explore the application of the 3D ZnO-NiO composite mesoporous architectures as electrochemical capacitors. Electrochemical study presents that the as-prepared 3D ZnO-NiO composites under different annealing conditions have different electrochemical supercapacitor properties. The as-synthesized sample obtained under 400 ^{o}C shows a high specific capacitance of 2498 F g^{-1} at a current density of 2.6 A g^{-1}, a good rate capability at high current densities and an excellent long-term cycling stability (about 3.0 % loss of the maximum specific capacitance after 2000 cycles), which is mainly attributed to its morphological characteristics of mesoporous and nanosheets self-assembling architectures, as well as a rational composition of the two constituents. These results suggest that such 3D ZnO-NiO mesoporous architectures are promising materials for the supercapacitor.

1. Introduction

In recent years, the design and preparation of the size, shape and morphology of desired nanostructured materials have received considerable interest for achieving novel morphology dependent chemical-physical properties and functionalities.[1-6] Specifically, porous nanostructures materials have attracted significant attention in the materials research fields due to their remarkable chemical and physical properties over their solid counterparts.[7-13] Because of the special porous features and specific surface area, such materials presented their prospects in various fields, such as energy storage, sensors, catalytic and environment protection.[14-23] Among porous materials with various morphologies, especially the higher-level 3D porous hierarchical structures materials, with high porosity and surface areas, have stimulated considerable attention for their unique properties compared with the respective individual low dimensional porous nanostructured materials and their respective non-porous structures.[24-34] Therefore, the development and synthesis of 3D porous hierarchical structures materials are important for their promising applications in many fields.

Sustainable energy research is attracting considerable attention as our planet is facing enormous environmental and energy challenges. Among the various technologies, electrochemical capacitors with a capacitance of thousands of Farads, namely supercapacitors (SCs), provide a potential route to solve energy storage problems because of their great advantages including exceptionally long cycle life, enhancing energy density, and high power density.[35-40]

Nickel oxide (NiO) is an important p-type wide-band gap oxide semiconductor. It has been a subject of considerable researches, and considered as one of promising materials in supercapacitive electrode materials due to its environmental compatibility, low cost, and high theoretical specific capacitance (2573 F g^{-1} within 0.5 V).[41-44] Despite these attractive features, such high theoretical specific capacitance has not been achieved experimentally owing to its poor electric conductivity. As one of the most attractive functional semiconductor materials, ZnO can be used as an efficient mechanical support and electron conducting pathway because of its high chemical stability, conductivity, and mechanical flexibility.[45] The individual physical and chemical properties of NiO or ZnO materials have been extensively studied, however there is few report on the ZnO-NiO composites for electrochemical capacitors.[46-49]

Recently, much attention has been focused on improving the specific capacitance of supercapacitors, via developing novel materials with rational design of mixed transition metal oxides and controllable 3D architectures, which can provide the synergistic effect of all individual constituents and efficient, rapid pathways for ion and electron transport not only at materials surfaces, but throughout the bulk of materials.[16, 49, 50-52] Although 3D architectures have been prepared for many simple metal oxides, the controllable preparation of mixed transition metal oxides with desirable composition and 3D architectures still remains a great challenge.[53-57] Thus, developing simple routes to prepare mixed transition metal oxides is very necessary. Thermal decomposition of nanostructured precursor compounds is usually used to synthesize mixed transition metal oxide powders. More importantly, when annealing nanostructured precursors, a large amount of gas can be released, resulting in a novel porous structure in the sample. In addition, the sample retains both the micro/nanoprecursors in addition to generating new porous structures.[16, 34, 49, 58 -60]

Herein, we have successfully prepared 3D hybrid ZnO-NiO mesoporous architectures via annealing the zinc hydroxide carbonate/nickel hydroxide carbonate composites precursors. These 3D architectures are assembled by hybrid ZnO-NiO.

mesoporous nanosheets. The specific 3D architecture has two advances: The one provides enough large inner space the other provides high active surface area due to a strong synergistic effect from ZnO and NiO. More importantly, as an electrode material for supercapacitors, the as-synthesized 3D hybrid ZnO-NiO composite architectures (**P1**, the detailed information seen in Materials preparation) show a high specific capacitance of 2498 F g^{-1}, a good rate capability at high current densities and an excellent long-term cycling stability (about 3.0 % loss of the maximum specific capacitance after 2000 cycles). Such 3D hybrid ZnO-NiO mesoporous architectures will be a promising electrode material for next generation supercapacitors.

2. Experimental Section

2.1 Materials preparation

In a typical procedure, 0.5 mmol $Zn(Ac)_2{\cdot}2H_2O$, 0.5 mmol $Ni(Ac)_2{\cdot}4H_2O$ and 2.0 mmol glycine were dissolved in 20 mL deionized water under vigorous stirring to form a clear solution. Then 2.0 mmol NH_4HCO_3 were added into the above solution under magnetic stirring. The resulting mixture solution was transferred into a 50 mL autoclave. The autoclave was sealed, heated at 180 ºC for 2 h and cooled down to room temperature naturally. The precipitate was collected by centrifugation and washed with distilled water and ethanol several times, then dried at 50 ºC for 12 h. Then the dry precipitate was calcined in the air at T = 400 ºC for 10 min, the heating-up rate was 1 ºC min^{-1}, the obtained product was denoted by P1. Products were obtained similarly, but with T = 450, and 550 ºC, which were denoted by correspond P2(450 ° C), and P3(550 ° C).

2.2 Electrode preparation

The work electrodes were prepared as follows: the electrode material of obtained 3D hierarchical porous ZnO-NiO composite was prepared according to the following steps. The mixture containing 80 wt% ZnO-NiO composites, 15 wt% acetylene black and 5 wt% polytetrafluoroethylene (PTFE) was well mixed, and then was pressed onto a nickel foam (1.2×10^7 Pa) that served as a current collector (the surface area was 1 cm^2). The typical mass load of electrode material was 5.0 mg.

2.3 Characterization

The morphology of as-prepared products was observed by a Hitachi S-4800 field emission scanning electron microscope (FE-SEM) at an acceleration voltage of 10.0 kV. The phase analyses of the samples were characterized by X-ray diffraction (XRD) on a Shimadzu XRD-6000 powder X-ray diffractometer with Cu-Kα radiation (λ = 1.5418 Å). Transmission electron microscopy (TEM) and high-resolution TEM (HRTEM) images were obtained on the JEOL JEM-2100 microscope at an acceleration voltage of 200 kV.

The electrochemical measurements were carried out by an electrochemical analyzer system, CHI660D (Chenhua, Shanghai, China) in a three-compartment cell with a platinum plate counter electrode, a saturated calomel electrode (SCE) reference electrode and a working electrode. The electrolyte was 3.0 M KOH aqueous solution. Electrochemical impedance spectroscopy (EIS) measurements were conducted at open circuit voltage in the frequency range of 100 kHZ to 0.01 Hz with an AC voltage amplitude of 5 mV using a PARSTAT 2273.

3. Results and Discussion

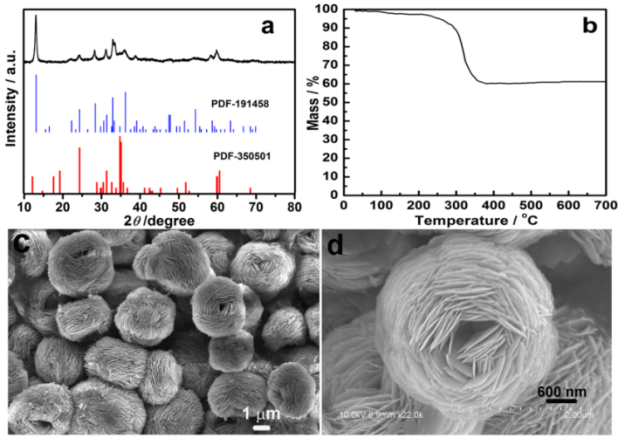

Fig. 1 (a) XRD pattern of the precursor; (b) TG curve of the precursor; and (c, d) SEM images of the precursor.

The hydrothermal synthesis process of the precursor was performed mildly. The powder X-ray diffraction pattern of the precursor is shown in Fig. 1a. All peaks are well in good agreement with the corresponding standard cards, JCPDS-35-0501 and 19-1458, for $Ni_2CO_3(OH)_2$ and $Zn_5(CO_3)_2(OH)_6$. The thermal behavior of the precursor samples has been investigated by TG analysis. As presented in Fig. 1b, the final temperature of thermal decomposion is about 400 ºC. SEM images of the precursor are shown in Fig. 1c, d. In Fig. 1c, the precursor formed 3D architectures with a size of about 2.0-3.0 μm. In Fig. 1d, the precursor architectures are composed of 2D nanosheets, which forms a 3D architecture with *ca*. 20 nm thickness of nanosheets .

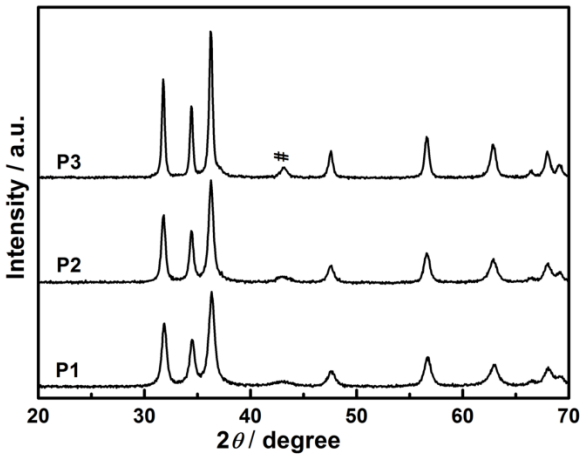

Fig. 2 XRD patterns of as-prepared ZnO-NiO composites (P1, P2 and P3).

The precursor was calcined at 400, 450 and 550 ºC to obtain ZnO-NiO composites (The obtained products were denoted by P1, P2 and P3, the detailed information seen in Materials preparation). The XRD pattern, Fig. 2, shows the phase structure of the ZnO-NiO composites. All diffraction peaks can be indexed to ZnO JCPDS-36-1451 except for the peak is marked by "#" which corresponds to NiO JCPDS-47-1049. The corresponding EDS mappings of the ZnO-NiO composites were also recorded (Fig.

S1-S3, ESI†) to further confirm the ratio of Zn and Ni elements. From Fig. S1-S3 (ESI†) three color mapping images, green: Ni-K, blue: Zn-K and red: O-K, are shown. For the different element contents, the green Ni-K color is much lighter than the blue Zn-K images, which reveals that the Ni content is much lower than the Zn content. Quantitative analysis of ratios of Zn and Ni elements for P1-P3 was also characterized. It found the Zn:Ni weight ratio of P1-P3 is 7:1in mass. X-ray photoelectron spectroscopy (XPS) studies also determine the chemical composition of the composites, Fig. 3. A survey scan shows the presence of the three elements (Ni, Zn and O) within the as-prepared hybrid ZnO-NiO materials. These results further demonstrate that the as-synthesized samples were hybrid ZnO-NiO materials.

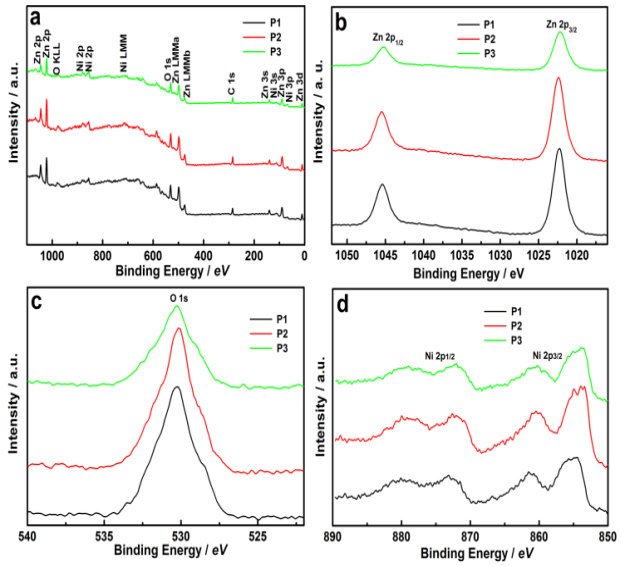

Fig. 3 (a) XPS survey scan of the ZnO-NiO composites; (b) Zn 2p; (c) O 1s, and (d) Ni 2p high resolution XPS spectra of P1-P3.

As seen from SEM images (Fig. 4), the morphology of the precursor was maintained in the prepared sample (P1) after calcinations in air, but surface of P1 has changed and become rough. P1 also has a porous 3D architecture with *ca*. 20 nm thickness of nanosheets (Fig. 4a-c). From Fig. 4d-f, P2 still consists of 3D architecture ZnO-NiO composites, which are composed of many nanosheets. After heating at 550 ºC for 10 min, P3 can be obtained, and the 3D architectures have been partially destroyed. The 3D architecture has shrunk during the thermal decomposition, and its building block nanosheets have fused together owing to the more extensive heating (Fig. 4g-i).

What's more, when calcining nanostructured precursors, a large amount of gas is released during the calcining process, resulting in a novel porous structure in the product. To further more obviously show the porous structures of the ZnO-NiO composite materials. TEM characterizations were performed on the products (Fig. 5). The apparent contrast between the white part and the black ligaments confirms the nanoporous wormhole-like characteristic (Fig. 5b, e). Up on further increasing in temperature, the building block particles of P3 have fused together. The pores of P3 have nearly disappeared because of the fusion of building blocks (Fig. 5h, i). An interplanar spacing of 0.28 nm corresponds to the separation between the (100) lattice planes of ZnO JCPDS-361451, and the other one spacing corresponding to the separation between the (200) lattice planes of NiO JCPDS-471049 (Fig. 5c, f and i).

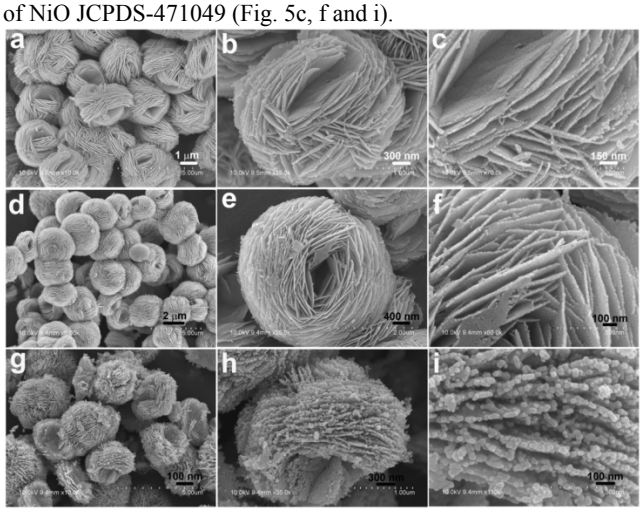

Fig. 4 SEM images of the as-prepared sample: (a, b, and c) P1; (d, e, and f) P2; (g, h, and i) P3.

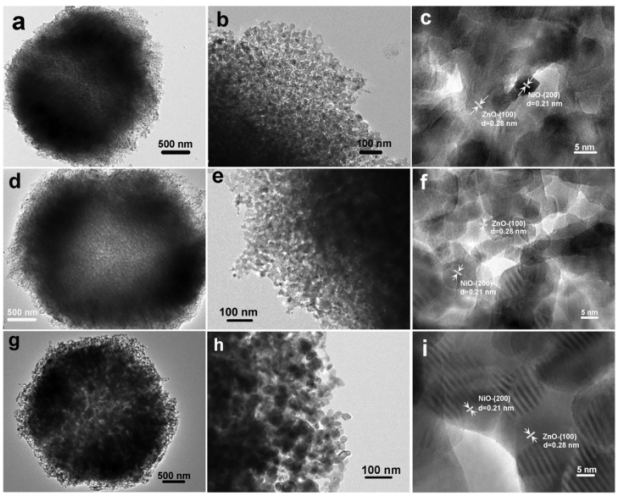

Fig. 5 TEM images of the 3D architectures ZnO-NiO composites: (a, b, and c) P1; (d, e, and f) P2; (g, h, and i) P3.

To gain further insight into the porous information and size distribution of products, Brunauer-Emmett-Teller (BET) measurements were characterized to examine their specific properties. The samples of P1 and P2 present a distinct hysteresis in the larger range *ca*. 0.75-1.0 P/P_0 in Fig. 6a, indicating the presence of mesopores possibly formed by porous stacking of component nanoparticles.[16, 61, 62] The BET surface area of P1 (48.4 $m^2 g^{-1}$) is much larger than that of P2 (34.3 $m^2 g^{-1}$) and P3 (12.6 $m^2 g^{-1}$), so allowing an efficient contact of activated materials with electrolytes or ions. The corresponding Barrett-Joyner-Halenda (BJH) pore size distribution curves (Fig. 6b) present that the average pore size is 14.4 nm, 24.9 nm and 80.4 nm for P1, P2 and P3, respectively. The porous structure of P1 leads to a high active surface areas and therefore efficient contact of P1 with the electrolyte.

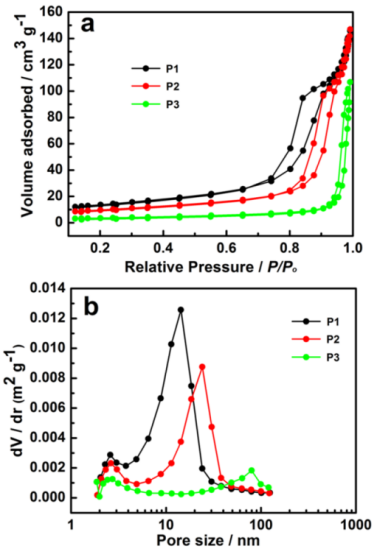

Fig. 6 N_2 adsorption-desorption isotherms of as-prepared samples; (b) Corresponding pore size distribution curves of as-prepared samples

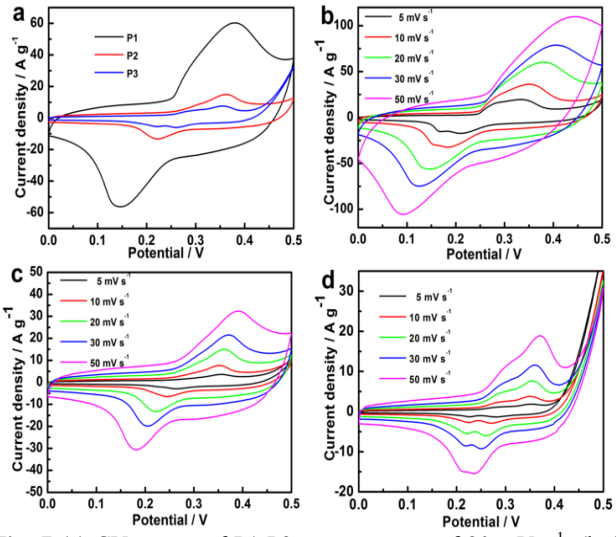

Fig. 7 (a) CV curves of P1-P3 at a scan rate of 20 mV s^{-1}; (b-d) cyclic voltammetry experiments within 0.0-0.5 V at a scan rate from 5.0 to 50 mV s^{-1} for P1-P3 electrodes in 3.0 M KOH electrolyte at room temperature.

It is well known that different micro/nanostructures might lead to different electrochemical conditions for ions intercalated/extracted into/out and electrolyte access. In order to determine the electrochemical capacitive properties of porous 3D architectures ZnO-NiO composite materials, cyclic voltammetry (CV) measurements in the range 0.00-0.50 V at scan rates from 5 to 50 mV s^{-1} were performed on the P1-P3 electrodes in 3.0 M KOH electrolyte at room temperature (Fig. **7**). For comparison, Fig 7a presents CV curves of P1-P3 at 20 mV s^{-1} in 3.0 M KOH electrolytes. The shapes of these curves are different from that of electric double-layer capacitance, suggesting that the capacity mainly results from pseudocapacitive capacitance. Furthermore, the shapes of the CV curves show that P1 has the biggest surrounded areas, indicating that the capacitance of P1 might be the largest one. The CV curves in Fig. 7d for P3 present smaller surrounded areas than those of P1 and P2, suggesting the poor electrochemical performance of P3.

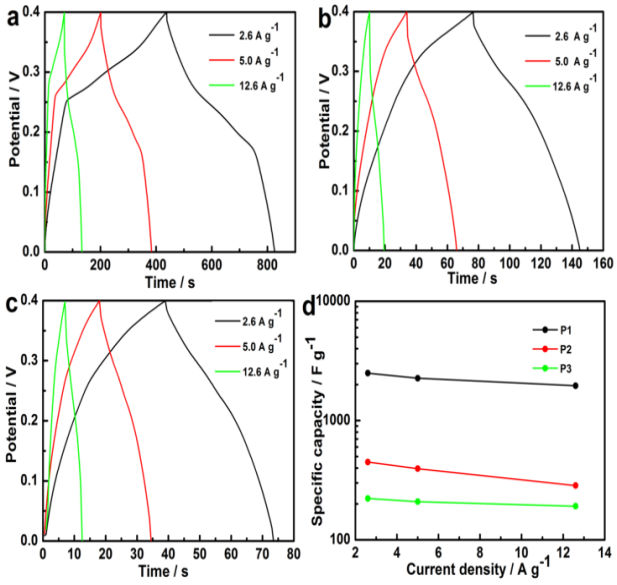

Fig. 8 (a-c) the galvanostatic charge-discharge curves of P1-P3 for current densities of 2.6, 5.0 and 12.6 A g^{-1} in 3.0 M KOH electrolyte at room temperature; (d) the specific capacitances calculated from the CP curves of P1-P3 at different current densities.

Rate capability is one of the important factors of evaluating the power applications of supercapacitors. The constant-current galvanostatic discharge measurements curves of P1-P3 are shown in Fig. 8 at different current densities of 2.6, 5.0 and 12.6 A g^{-1} in 3.0 M KOH electrolytes. The specific capacitance of an electrode during galvanostatic charge/discharge can be calculated from eq. (1):[16, 33]

$$C = (I\,\Delta t)/(m\,\Delta V) \qquad (1)$$

Where C (F g^{-1}), and I is the discharge current (A) applied for time Δt (s), m is the mass of activated materials (g), ΔV is the range of charge/discharge (V).

The specific capacitances derived from the discharging curves at current densities of 2.6-12.6 A g^{-1} are shown in Fig. 8d. From discharging curves, the specific capacitances are 2497.8 F g^{-1} (P1), 449.3 F g^{-1} (P2) and 222.4 F g^{-1} (P3) at 2.6 A g^{-1} in 3.0 M KOH solution. At a high current density of 12.6 A g^{-1}, the specific capacitance of P1 remained at 1959.1 F g^{-1}, while that of P2 and P3 are reduced to 285.5 and 191.6 F g^{-1}. Furthermore, compared with other values, the specific capacitance of P1 is significantly better than some nickel based nanomaterials, such as NiO nanospheres (2 A g^{-1}, 803 F g^{-1}), NiO nanospindles (10 A g^{-1}, 1200 F g^{-1}), mesoporous NiO (3 A g^{-1}, 345 F g^{-1}), NiO nanoflowers (5 A g^{-1}, 252 F g^{-1}).[63-66] As we all known, ions diffusion and electron transport play two important roles in the performance of supercapacitor. Commonly, it is believed that the materials with porous structure should be better in energy storage for the higher surface area and the channels for ions diffusion. In addition, if nanopore is completely coated with an electronic conductive layer-carbon additive, the electronic transport length in an electrode would be effectively shortened. Thus, such superior an excellent rate capability of P1 may be attributed to short ion diffusion and electron transport path within the 3D architectures assembled by many interconnecting porous

nanosheets.[33, 67]

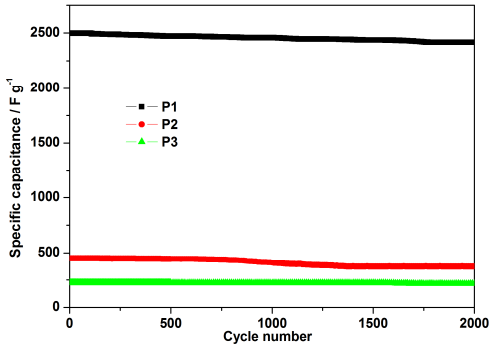

Fig. 9 Charge/discharge cycling test at 2.6 A g^{-1}.

Fig. 9 presents the specific capacitance retentions of the P1-P3 sample electrodes as a function of charge/discharge cycling numbers. We find that all the electrodes have good cycle life. Especially, the curve of P1 shows its good specific capacitance retention at a current density of 2.6 A g^{-1} in 3.0 M KOH solution. The P1 electrode showed only 3.0 % loss of the specific capacitance after 2000 continuous charge-discharge cycles, while those of P2 and P3 maintained 83.2% and 96.4%, illustrating the good long-term cyclability of the P1 electrode.

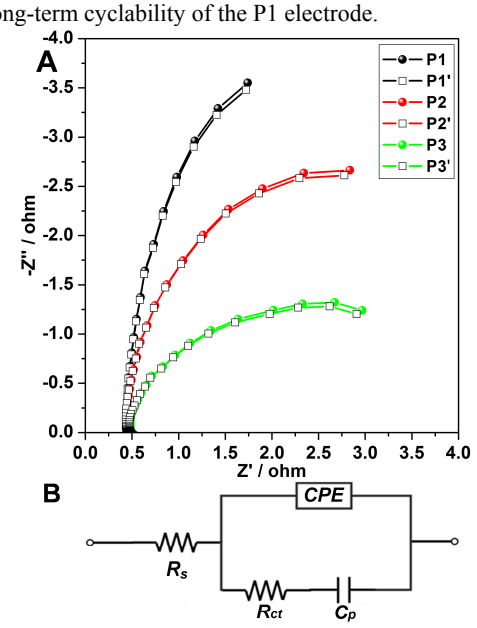

Fig. 10 (A) Electrochemical impedance spectra (EIS) for P1, P2, and P3 nanostructured electrodes under room temperature in 3.0 M KOH solutions and corresponding fitted curves (P1', P2', and P3') by ZSimpWin software; (B) An equivalent circuit an consisting of a bulk solution resistance R_s, a charge-transfer R_{ct}, a pseudocapacitive element C_p from redox process of P1, P2, and P3 nanomaterials, and a constant phase element (CPE) to account for the double-layer capacitance.

To identify the exact electrical conductivity of electrodes, we have measured EIS spectrum of P1, P2, and P3 nanostructured electrodes at room temperature in the frequency range 0.01–10^5 Hz under open-circuit conditions, which are shown in Fig. 10A. An equivalent circuit used to fit the impedance curve is given in Fig. 10B, similar to the circuit which is employed as the working electrode of supercapacitor. The EIS spectrum can be fitted by a bulk solution resistance R_s, a charge-transfer R_{ct} and a pseudocapacitive element C_p from redox process of electrode materials, and a *CPE* to account for the double-layer capacitance. The corresponding fitted curves (P1', P2', and P3') by ZSimpWin software based on the proposed circuit are also shown Fig. 10A. What's more, the charge-transfer resistances R_{ct} of all the samples were calculated by ZSimpWin software, and from the calculated results in **Table 1**, we found that P1 electrodes have the lowest value-1.7 Ω, and detailed others R_{ct} values (P2-3.6 Ω and P3-7.8 Ω). It clearly demonstrates the reduced charge-transfer resistance of the P1 electrode. In addition, the charge-transfer resistance R_{ct}, also called Faraday resistance, is a limiting factor for the specific power of the supercapacitor. It is the low Faraday resistance that results in the high specific power of P1 electrode. This P1 nanostructured surface-interface character might also decrease the polarization of the electrode, and thus increase the capacity.

Table 1 Calculated values of R_s, *CPE*, R_{ct}, and C_p of the supercapacitor electrodes consisting of P1, P2 and P3 through fitting of the experimental impedance spectra based on the proposed circuit in Fig. 10B.

Samples	R_s/ohm	*CPE*/mF	R_{ct}/ohm	C_p/F
P1	0.45	0.60	1.7	1.10
P2	0.45	0.34	3.6	0.78
P3	0.46	0.12	7.8	0.71

It is found that 3D ZnO-NiO architectures formed at different temperature thermal treatment have different supercapacitor performance in this paper. The difference in electrochemical performance of the 3D ZnO-NiO architectures can be explained as followings. First, such superior electrochemical performance in P1 might be attributed to the highly accessible surface area, good conductivity and special 3D hierarchical structures. From BET measurements of the mesoporous 3D ZnO-NiO architectures, we find that the BET surface area of P1 is much larger than that of P2 and P3. Therefore, P1 can offer large electrode/electrolyte contact area and short diffusion path for ions. We conclude that the conductivity of materials play an important role in electrochemical properties, and the sequence of conductivity is P1>P2>P3. And, the 3D ZnO-NiO mesoporous hierarchical structures are beneficial for electrolyte transport, allowing full contact of the activated materials with OH^{-1} in the electrolyte, thus increasing the utilization of activated materials.[68, 69] Second, although the ZnO-NiO composites have a small amount of NiO, ZnO and NiO can easily form p-n heterostructure, the formation of the heterostructure between ZnO and NiO nanocrystals generate an enhanced inner electric field in the interface of ZnO and NiO nanoparticles, which may improve the electron transfer between nanoparticles, [70, 71] Different surface/interface characteristics and conductivity will lead to different chemical–physical adsorption–desorption abilities towards ions and diffusion path of ions, resulting in different electrochemical performance of P1–P3.

4. Conclusions

In summary, novel 3D hybrid ZnO-NiO mesoporous architectures have been synthesized through a simple route. We have successfully explored the application of the 3D hybrid ZnO-NiO composite architectures as electrochemical capacitors. The porous 3D hybrid ZnO-NiO architectures enable a fast and reversible redox reaction to improve the specific capacitance, especially for the P1 which can effectively transport electrolytes and shorten the ion diffusion path. Such porous 3D hybrid ZnO-NiO architectures are promising materials for next generation supercapacitors.

Acknowledgements

This work is supported by the Program for New Century Excellent Talents from the ministry of education (**NCET**-13-0645) and National Natural Science Foundation of China (**NSFC**-21201010), the Science & Technology Foundation of Henan Province (122102210253, 13A150019), the China Postdoctoral Science Foundation (2012M521115)，and the opening research foundations of State Key Laboratory of Coordination Chemistry

Notes and references

[a] *College of Chemistry and Chemical Engineering, Anyang NormalUniversity, Anyang, 455000 Henan, P. R. China. E-mail: huanpangchem@hotmail.com*

[b] *State Key Laboratory of Coordination Chemistry, Nanjing University, Nanjing, 210093 Jiangsu, P. R. China.*

1 M. H. Cao, T. F. Liu, S. Gao, G. B. Song, X. L. Wu, C. W. Hu and Z. L. Wang, *Angew. Chem., Int. Ed.*, 2005, **44**, 4197.

2 J. Y. Zhong, C. B. Cao, Y. Y. Liu, Y. N. Li and W. S. Khan, *Chem. Commun.*, 2010, **46**, 3869.

3 B. Wang, J. S. Chen and X. W. Lou, *J. Mater. Chem.*, 2012, **22**, 9466.

4 X. L. Hu and J. C. Yu, *Adv. Mater.*, 2008, **18**, 880.

5 J. P. Liu, X. T. Huang, Y. Y. Li, K. M. Sulieman, X. He and F. L. Sun, *Cryst. Growth Des*, 2006, **6**, 1690.

6 X. F. Li, Y. H. Hu, J. Liu, A. Lushington, R. Y. Li and X. L. Sun, *Nanoscale*, 2013, **5**, 12607.

7 Z. Y. Wang, Z. C. Wang, H. B. Wu and X. W. Lou, *Sci Rep*, 2013, **3**, 1391.

8 F. M. Zhan, B. Y. Geng and Y. J. Guo, *Chem.- Eur. J.*, 2009, **15**, 6169.

9 B. Y. Geng, F. M. Zhan, C. H. Fang and N. Yu, *J. Mater. Chem.*, 2008, **18**, 4977.

10 Y. Qiao, X. L. Hu, Y. Liu, G. Liang, M. C. Croft and Y. H. Huang, *J. Mater. Chem. A.*, 2013, **1**, 15128.

11 C. Z. Yuan, S. L. Xiong, X. G. Zhang, L. F. Shen, F. Zhang, B. Gao and L. H. Su, *Nnao Res.*, 2009, **2**, 722.

12 Y. G. Wang, L. Cheng, F. Li, H. M. Xiong and Y. Y. Xia, *Chem. Mater.*, 2007, **19**, 2095.

13 W. Luo, X. L. Hu, Y. M. Sun and Y. H. Huang, *ACS Appl. Mater. Interfaces*, 2013, **5**, 1997.

14 L. Zhou, D. Y. Zhao and X. W. Lou, *Adv. Mater.*, 2012, **24**, 745.

15 C. Guan, X. L. Li, Z. L. Wang, X. H. Cao, C. Soci, H. Zhang and H. J. Fan, *Adv. Mater.*, 2012, **24**, 4186.

16 H. Pang, J. W. Deng, J. M. Du, S. J. Li, J. Li, Y. H. Ma, J. S. Zhang and J. Chen, *Dalton Trans.*, 2012, **41**, 10175.

17 E. S. Toberer, T. D. Schladt and R. Seshadri, *J. Am.* Chem. Soc., 2006, **128**, 1462.

18 M. Han, M. Fang, L. L. Liu, J. C. Bao and Z. H. Dai, *Electrochem. Commun.*, 2013, **35**, 94.

19 G. X. Wang, X. L. Gou, J. Horvat and J. Park, *J. Phys. Chem. C*, 2008, **112**, 15220.

20 Y. F. Yu, Y. M. Zhu and M. Meng, *Dalton Trans.*, 2013, **42**, 12087.

21 J. X. Zhu, Z. Y. Yin, H. Li, H. T. Tan, C. L. Chow, H. Zhang, H. H. Hng, J. Ma and Q. Y. Yan, *Small*, 2011, **7**, 3458.

22 W. Wang, H. Y. Wang, W. Wei, Z. G. Xiao and Y. Wan, *Chem.-Eur. J.*, 2011, **17**, 13461.

23 Z. C. Bai, B. Sun, N. Fan, Z. C. Ju, M. H. Li, L. Q. Xu and Y. T. Qian, *Chem. Eur. J.*, 2012, **18**, 5319.

24 Z. J. Xing, B. Y. Geng, X. L. Li, H. Jiang, C. X. Feng and T. Ge, *CrystEngComm*, 2011, **13**, 2137.

25 X. H. Zhang, Y. N. Li and C. B. Cao, *J. Mater. Chem.*, 2012, **22**, 13918.

26 G. X. Zhu, H. Xu, Y. Y. Xiao, Y. J. Liu, A. H. Yuan and X. P. Shen, *ACS Appl. Mate. Interfaces*, 2012, **4**, 744.

27 C. Z. Yuan, X. G. Zhang, L. H. Su, B. Gao and L. F. Shen, *J. Mater. Chem.*, 2009, **19**, 5772.

28 H. Pang, C. Z. Wei, Y. H. Ma, S. S. Zhao, G. C. Li, J. S. Zhang, J. Chen and S. J. Li, *ChemPlusChem*, 2013, **78**, 546.

29 H. B. Wu, H. Pang and X. W. Lou, *Energy Environ. Sci.*, 2013, 6, 3619.

30 H. Pang, F. Gao, Q. Chen, R. M. Liu and Q. Y. Lu, *Dalton Trans.*, 2012, **41**, 5862.

31 G. X. Zhu, C. Y. Xi, H. Xu, D. Zheng, Y. J. Liu, X. Xu and X. P. Shen, *RSC Adv.*, 2012, **2**, 4236.

32 G. G. Wang, X. F. Wang, J. F. Liu and X. M. Sun, *Chem.-Eur. J.*, 2012, **18**, 5361.

33 H. Pang, Z. Yan, Y. Wei, X. Li, J. Li, L. Zhang, J. Chen, J. Zhang and H. Zheng, *Part. Part. Syst. Charact.*, 2013, **30**, 287–295.

34 K. B. Xu, R. J. Zou, W. Y. Li, Y. F. Xue, G. S. Song, Q. Liu, X. J. Liu and J. Q. Hu, *J. Mater. Chem. A.*, 2013, **1**, 9107.

35 J. Jiang, Y. Y. Li, J. P. Liu, X. T. Huang, C. Z. Yuan and X. W. Lou, *Adv. Mater.*, 2012, **24**, 5166.

36 C. Z. Yuan, B. Gao, L. F. Shen, S. D. Yang, L. Hao, X. J. Lu, F. Zhang, L. J. Zhang and X. G. Zhang, *Nanoscale*, 2011, **3**, 529.

37 X. F. Xia, Q. L. Hao, W. Lei, H. L. Wang and X. Wang, *J. Mater. Chem.*, 2012, **22**, 8314.

38 M. Winter and R. J. Brodd, *Chem. Rev.*, 2004, **104**, 4245.

39 Y. Gogotsi and P. Simon, *Science*, 2011, **334**, 917.

40 H. C. Chien, W. Y. Cheng, Y. H. Wang and S. Y. Lu, *Adv. Funct. Mater.*, 2012, **22**, 5038.

41 C. Y. Cao, W. Guo, Z. M. Cui, W. G. Song and W. Cai, *J. Mater. Chem.*, 2011, **21**, 3204.

42 B. Wang, J. S. Chen, Z. Y. Wang, S. Madhavi and X. W. Lou, *Adv. Energy Mater.*, 2012, **2**, 1188.

43 Q. Li, Y. J. Chen, T. Yang, D. N. Lei, G. H. Zhang, L. Mei, L. B. Chen, Q. H. Li and T. H. Wang, *Electrochim. Acta*, 2013, **90**, 80.

44 Z. H. Yang, F. F. Xu, W. X. Zhang, Z. S. Mei, B. Pei and X. Zhu, *J. Power Sources*, 2014, **246**, 24.

45 Y. B. He, G. R. Li, Z. L. Wang, C. Y. Su and Y. X. Tong, *Energy Environ. Sci.*, 2011, **4**, 1288.

46 H. Ohta, M. Hirano, K. Nakahara, H. Maruta, T. Tanabe, M. Kamiya, T. Kamiya and H. Hosono, *Appl. Phys. Lett.*, 2003, **83**, 1029.

47 X. Z. Wang, W. Liu, J. R. Liu, F. L. Wang, J. Kong, S. Qiu, C. Z. He and L. Q. Luan, *ACS Appl. Mater. Interfaces*, 2012, **4** ,817.

48 Q. Pan, L. Qin, J. Liu and H. Wang, *Electrochim. Acta*, 2010, **55**, 5780.

49 H. Pang, Y. H. Ma, G. C. Li, J. Chen, J. S. Zhang, H. H. Zheng and W. M. Du, *Dalton Trans.*, 2012, **41**, 13284.

50 J. P. Liu, J. Jiang, M. Bosman and H. J. Fan, *J. Mater. Chem.*, 2012, **22**, 2419.

51 J. K. Chang, M. T. Lee, C. H. Huang and W. T. Tsai, Mater. *Chem. Phys.*, 2008, **108**, 124.

52 H. Chen, L. F. Hu, Y. Yan, R. C. Che, M. Chen and L. M. Wu, *Adv. Energy Mater.*, 2013, **3**, 1636.

53 H. B. Wu, X. W. Lou and H. H. Hng, *Chem.- Eur. J.*, 2012, **18**, 2094.

54 B. Wang, J. S. Chen, H. B. Wu, Z. Y. Wang and X. W. Lou, *J. Am. Chem. Soc.*, 2011, **133**, 17146.

55 A. M. Cao, J. S. Hu, H. P. Liang and L. J. Wan, *Angew. Chem., Int. Ed.*, 2005, **44**, 4391.

56 M. H. Cao, X. Y. He, J. Chen and C. W. Hu, *Cryst. Growth Des*, 2007, **7**, 170.

57 J. B. Fei, Y. Cui, X. H. Yan, W. Qi, Y. Yang, K. W. Wang, Q. He and J. B. Li, *Adv. Mater.*, 2008, **20**, 452.

58 L. Zhang, H. B. Wu and X. W. Lou, *J. Am. Chem. Soc.*, 2013, **135**, 10664.

59 Q. S. Xie, H. Z. Guo, X. X. Zhang, A. L. Lu, D. Q. Zeng, Y. Z. Chen,

and D. L. Peng, *RSC Adv*., 2013, **3**, 24430.
60 C. C. Kuo, W. J. Lan and C. H. Chen, *Nanoscale*, 2014, DOI: 10.1039/C3NR03791F.
61 X. F. Zhou, Z. L. Hu, Y. Q. Fan, S. Chen, W. P. Ding and N. P. Xu, *J. Phys*. *Chem*. *C*, 2008, **112**, 11722.
62 J. Y. Baek, H. W. Ha, I. Y. Kim and S. J. Hwang, *J. Phys*. *Chem*. *C*, 2009, **113**, 17392.
63 D. T. Dam and J. M. Lee, *Electrochim*. *Acta*, 2013, **108**, 617.
64 H. Pang, B. Zhang, J. M. Du, J. Chen, J. S. Zhang and S. J. Li, *RSC Adv*., 2012, **2**, 2257.
65 S. L. Xiong, C. Z. Yuan, X. G. Zhang and Y. T. Qian, *CrystEngComm*, 2011, **13**, 626.
66 S. I. Kim, J. S. Lee, H. J. Ahn, H. K. Song and J. H. Jang, *ACS Appl*. *Mater*. *Interfaces*, 2013, **5**, 1596.
67 H. Pang, C. Z. Wei, X. X. Li, G. C. Li, Y. H. Ma, S. J. Li, J. Chen and J. S. Zhang, *Sci*. *Rep*., 2014, **4**, 3577.
68 H. Jiang, T. Zhao, C. Z. Li and J. Ma, *J. Mater. Chem.*, 2011, **21**, 3818.
69 J. P. Liu, C. W. Cheng, W. W. Zhou, H. X. Li and H. J. Fan, *Chem. Commun.*, 2011, **47**, 3436.
70 L. Xu, R. F. Zheng, S. H. Liu, J. Song, J. S. Chen, B. Dong and H. W. Song, *Inorg. Chem.*, 2012, **51**, 7733.
71 L. J. Lauhon, M. S. Gudiksen, D. Wang and C. M. Lieber, *Nature*, 2002, **420**, 57.